A Comprehensive High-Level Model for CMOS-MEMS Resonators

Saoni Banerji, Daniel Fernández, and Jordi Madrenas

***Abstract*— This paper presents a behavioral modeling technique for CMOS-MEMS microresonators that enables simulation of a MEMS resonator model in Analog Hardware Description Language (AHDL) format within a system-level circuit simulation. A 100 kHz CMOS-MEMS resonant pressure sensor has been modeled into Verilog-A code and successfully simulated within Cadence framework. Analysis has shown that simulation results of the reported model are in agreement with the device characterization results. As an application of the proposed methodology, simulation and results of the model together with an integrated monolithic low-noise amplifier is exemplified for detecting the position change of the resonator.**

***Index Terms*— Co-simulation, CMOS-MEMS, microresonators, behavioral modeling, AHDL**

I. Introduction

The significant growth we see today in the microelectromechanical systems (MEMS) sensor market is fueled mainly by one thing: the increasing demand of wearables, human-interface devices (HID) and applications by the end consumer. Besides the main design driving forces of size and integration, typical of the wearable market [1] (smart watches, mobile phones, smart rings, etc.), the time-to-market has become a critical engineering factor. As engineers are pushed towards shorter and shorter design cycles, quick design simulation and verification is a key factor.

The design complexity of wearables, involving in many cases the monolithic integration of several key blocks (sensor, analog conditioning and system processing), requires advanced simulation tools to ensure compatibility among the parts, hence, a co-simulation of the different domains is necessary. While between the analog/digital blocks, co-simulation is well supported with all the major microelectronics design tools, the MEMS sensor block requires very specific tools for simulation that can account for several physical effects, including air damping, mechanical motion, capacitive detection and electrostatic actuation. Those are all co-dependent, hence requiring careful investigation.

The ideal co-simulation design tool for MEMS-electronics integration should support theoretical characterization of devices before design, manufacturing and prototyping,

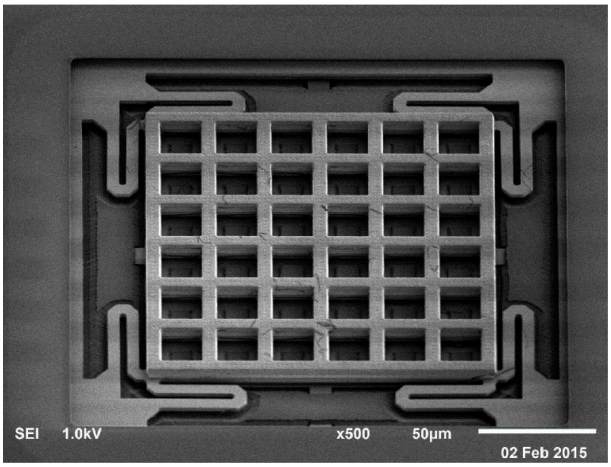

Fig. 1. Scanning Electron Microscope (SEM) micrograph of the fabricated CMOS pressure sensor.

allowing to determine the key specification parameters together with the electronics. This would allow starting the design of both the electronics and the MEMS at the same time, hence shortening the design cycle and reducing the time-to-market. Also, the tool is also expected to be able to handle mixed-domain simulation, specifically the co-simulation with transistor-level electronics. This is due to the importance of the consideration of large number of interactions in the mechanical and electrical domain; critical for analyzing the performance of MEMS [2]. Accurate capture of the performance of electronics and interaction with MEMS transducers is highly demanded owing to the increased complexity of MEMS, which cannot be fulfilled by simple electrical component models [3].

Existing simulation methodologies include finite and boundary element analyses (FEA/BEA) for numerical, electrostatic and mechanical simulations. [4]-[5]. The commercially available tools used for MEMS design community include ANSYS, Comsol Multiphysics, Coventorware and ABAQUS. Creation of system matrix for both mechanical and electrostatic FEA has extended their capability in providing multi-physics simulations. Despite their capability of defining fine meshes for structures, owing to their

[1] An earlier reduced version of this paper was presented at the IEEE Sensors 2016 Conference in Orlando, Florida.

This work has been partially funded by the Spanish Ministry of Science and Innovation and the European Social Fund (ESF) under Project TEC2015-67278-R. Saoni Banerji holds an FI scholarship funding by the Catalan government and European Social Fund (ESF).

Saoni Banerji and Daniel Fernández are with Nanusens, CENT-Parc Tecnològic del Vallès, Av. del Parc Tecnològic, 3, 08290 Cerdanyola Del Vallès, Spain.

Jordi Madrenas is with Electronic Engineering Department, Universitat Politècnica de Catalunya, Jordi Girona 1-3, 08034 Barcelona, Spain.

layout-based dependency, any change in the device geometry would require a new mesh. This does not allow convenience in design iterations. Besides, they fail to fulfil the co-simulation between the transducers and transistor-level interface circuits. As a result, designers faced with difficulties in predicting the performance of system-level simulations with external CMOS circuitry [6].

A vast number of approaches were hereafter established to find robust methods to perform nonlinear macro modeling. Reduced order modeling enhances system simulation time and meets the requirement of co-simulation with electronics. There has been an widespread adoption of Verilog-A as the de facto language for defining compact models for circuit simulation [7]. Prior works have investigated on the initiation of the modeling approach of resonators [8]-[9] where a Finite Element Model (FEM) is transformed into an Analog Hardware Description Language (AHDL) model. A method for creating a fully non-linear device model has been reported in [10] which can be used as a black box for a 10-MHz clamped-clamped beam resonator reported as a test case in [11]. A subsequent simulation and inclusion of a similar model have been reported to show the plausibility of functionality of a MEMS resonator with an external electronic circuitry [12]. However, as the models are based on a prioritized motion shape subset, they are only valid for specific structures which would require re-creation of new models in case of alteration of device topology[2]. Circuit-level behavioral nodal simulations using NODAS tools have been proposed to have an advantage of easing iterative design evaluation and capability to simulate other oscillation modes [2]. However, they suffer from a disadvantage of increased simulation time.

The present paper discusses the design space of CMOS-MEMS resonators for two reasons: First, resonators form one of the simplest suspended MEMS devices (all the movable parts of a device are suspended by springs attached to fixed anchor points). Secondly, CMOS-MEMS, unlike other MEMS areas (i.e. Microfluidics and BioMEMS), require tight integration with electronics in larger System-on-Chip (SoC) devices. Moreover, the design of resonator electronics demands for good accuracy, fast speed, ability to handle complexity and ease of iterative evaluation during the design cycle. Owing to the capability of the reduced simulation time and ability of geometrical parametrization, models written in Verilog-A and simulated within the Cadence framework simplify the evaluation microelectronics design topologies, thus allowing multiple design iterations without losing accuracy in the mechanical-electrical interaction.

This paper presents a comprehensive guide to the modeling and simulation methodology of a CMOS-MEMS resonator in Verilog-A within Cadence framework. In Section II, a second order non-linear behavioral model, targeted to emulate the real-time behavior of a prior reported CMOS-MEMS resonator [13] is introduced. The model is written in Verilog-A and the simulations are performed within the Cadence framework, allowing co-simulation of MEMS with electronics. The model includes the Brownian noise and the non-linearity such as the Duffing effect, as well as thermal effects in the gap and elastic constants, and statistical variations due to mismatch. In Section III, the model parameters are aligned with the device measurements to verify and validate the model accuracy, and the results are presented. In Section IV, other key aspects about the model, required for proper functioning in the Cadence framework are presented. As a final example, in Section V the model is used within a co-simulation environment together with an integrated monolithic low-noise amplifier for detecting the position change of the resonator. This is followed by concluding remarks in Section VI.

II. High-Level Model for CMOS-MEMS Resonator

As a guiding example for the high level non-linear model extraction, a prototype pressure sensor operating as a resonator has been used. The pressure sensor, shown in **Fig. 1** has been designed with an optimal geometry of 140 × 140 × 8 µm having 6 × 6 perforations along the row and column of the plate, respectively, for maximum Q, with an effective mass of 0.4 µg. An enhanced quality factor of 60 and reduced damping coefficient of 4.34 µNs/m have been obtained for the reported device at atmospheric pressure [13]-[17]. The reported capacitive pressure sensor, fabricated using IHP SG25 process, is implemented as a two aluminum layers (with a thickness of 2 µm and 3 µm) separated by a 3 µm thick tungsten via [13]. The pressure sensor was manufactured in 250 nm CMOS technology, and the release was performed at the dice level in the UPC-DEE cleanroom with a hydrogen fluoride etchant to release the back-end of line (BEOL) metal layers. The details of the release procedure are mentioned in [20]-[21].

First, we will begin the model design with a reduction of the MEMS resonator structure to a second-order mechanical system. Then, we will calculate, step by step, all the forces applied over the membrane, i.e. the electrical force, the linear mechanical restoration force and the damping. We will add then the effects of temperature and nonlinear mechanical effects to the model and finally the Brownian noise and mismatch manufacturing variations.

Throughout this section, we have shown key sections of the model to show how the governing equations have been implemented. The parameters used in the model have been tabulated in **Table I** to ease the understanding of the equations.

A. Second-order model reduction and determination of the electrical force

The schematic of a resonator that emulates the pressure sensor in [12] is shown in **Fig. 2**.

It has been modeled as a two-plate device in Verilog-A with a movable flexural membrane separated by an on-rest gap z_0 over a fixed substrate. When voltage is applied over the movable membrane i.e. the capacitance, attached to a spring k;

TABLE I
SYMBOLS USED IN THE VERILOG-A MODEL

Model parameters			
Symbol	**Value**	**Meaning**	**Units**
Q_lin	4754	Linear term of the Q vs. temperature and pressure equation	
QPow_P	-0.4771	Exponent of the Q vs. pressure equation	[]
QPow_T	-0.9	Exponent of the Q vs. temperature equation	[]
k_1	170	Spring constant of the movable plate	N/m
k_3	-1×10^{-12}	Non-linear coefficient of the spring constant	N/m^3
k_tc	-0.113	Temperature coefficient of the spring constant	N/(mºC)
k_mean	153	Average spring constant of the movable plate	N/m
k_std	25.19	Standard deviation of the spring constant	N/m
m	3.88×10^{-10}	Mass of the movable plate	kg
area	18×10^{-9}	Area of the plate	m^2
precision_factor	4	Accuracy of simulation (Typical value of 4 gives good results)	[]
mismatch	0	If zero, the simulator computes a nominal simulation. Otherwise, it performs a statistical simulation.	[]
gap_initial	0	Initial position of the movable plate	m
gap_mean	2.55×10^{-6}	Average distance between the plates	m
gap_tc	0	Temperature coefficient of the distance between the plates	m
gap_min	0.01×10^{-6}	Distance between the stoppers of the movable plate and the actuation plate	m
gap_std	1	Standard deviation from the average value of the distance between plates	m
def_corr	1	Correction factor applied to the forces to account for the deformation of the plates	[]
Model inputs			
Symbol	**Value**	**Meaning**	**Units**
Pressure	101325	Applied ambient pressure	Pa
ext_force	0	External force	N
ext_accel	0	External acceleration	m/s^2
PLDN	10	Voltage of fixed electrode	V
PLATE	10	Voltage of the movable plate	V
Model outputs			
Symbol	**Value**	**Meaning**	**Units**
position	-	Position of the movable plate (Position = 0 on rest)	m
C_res	-	Capacitance between the plates	F
aux	-	For testing/debugging	[]
Q_fac	-	Quality factor of the resonator	[]

an electrostatic force works to reduce the plate separation to z_0-z, where z is the distance traversed by the movable membrane and z_0 is the on-rest distance between the movable membrane and fixed substrate. This is incorporated in the model as a start to the working principle of a resonator [2] expressed as

$$C = \frac{\varepsilon A}{z_0 - z} \quad (1)$$

where C is the capacitance between the parallel plates and A is the area of the movable plate.

The resonator capacitance is expressed in terms of the ability of the device to store an electric charge [3]

$$Q = CV \quad (2)$$

[2] C(C_res) <+ area*`P_EPS0/(gap_val+position_val); // Capacitance estimation.
[3] Q(charge) <+ C(C_res)*(V(PLDN)-V(PLATE)); // Definition of charge.

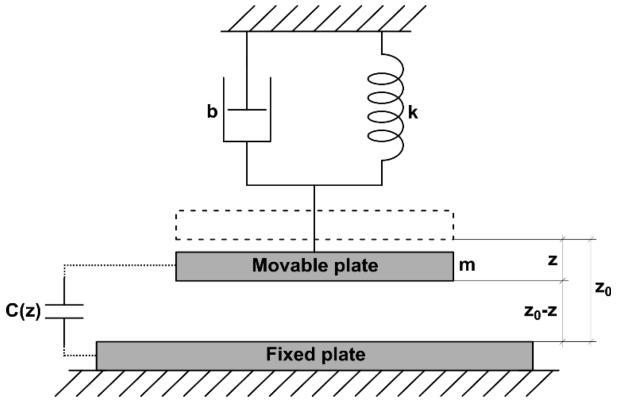

Fig. 2. Lumped model of the two plate CMOS-MEMS Resonator

While, the current drained by the resonator between the two plates can be expressed as a derivative of an electric charge Q [4].

$$I = \frac{\partial Q}{\partial t} \tag{3}$$

This electrostatic force acting on the movable plate can be expressed as [5] [16]

$$F = \frac{-Q^2}{2\varepsilon A} \tag{4}$$

The second-order differential equation for the lumped resonator model, in terms of the nonlinear spring force, can be expressed as

$$m\ddot{z} + b\dot{z} + k_1 z \quad = \sum F_{ext} \tag{5}$$

where $\sum F_{ext}$ is the summation of external forces applied to the resonator, m is the effective mass, b is the net damping coefficient, and k_1 is the linear spring constant. Here z, $\dot{z}$, $\ddot{z}$ are the displacement, velocity, and acceleration of the system respectively [12]. Equation (5) has been fragmented into several parts, discussed in this section and have been implemented in the model, depending on the factors that affect the device operation. These forces have been implemented in the model as [6],[7],[8], respectively. The calculation of the values is explained in the next subsection.

B. Effects of damping and temperature

It is worth to note that the device of a resonating pressure sensor is primarily dependent on the viscosity of the surrounding fluid i.e. air, in regimes where air damping is the dominant loss mechanism. Through the equations implemented in the model, we can observe that the second term in Equation (5) is expressed in terms of the device damping coefficient. We should note that the damping coefficient of the device can be expressed in terms of the resonator Q, which measures the energy loss from the resonator and evaluates the device performance.

$$b = \frac{2\pi m f_r}{Q} \tag{6}$$

where m is the effective mass of the resonator, f_r is the resonance frequency and b is the damping coefficient of the device. Equation (6) can be substituted in Equation (5) and re-written as

$$m\ddot{z} + \left(\frac{2\pi m f_r}{Q}\right)\dot{z} + k_1 z \quad = \sum F_{ext} \tag{7}$$

The second term in Equation (7) contributing to the electrical force is represented in [7]. At constant temperature, the quality factor Q follows a power function with the air pressure P_a than can be expressed as

$$Q = a(P_a)^b \tag{8}$$

where a and b are coefficients relating Q to pressure [12].

Temperature disturbance is another vital concern in the field of resonant sensors. They can lead to frequency drift owing to the stress changes [18]-[22], and its effect of temperature on the resonator spring constant is incorporated in the model [8]. The trend of variation of Q with temperature T, at constant pressure for the reported device has been analyzed and can be modeled on first approximation as

$$Q = c(T)^{\gamma} \tag{9}$$

where c is a constant scaling factor and γ represents a coefficient that characterizes the reverse temperature dependence on Q, signified by Knudsen number (Kn) and the dominant damping mechanisms in every pressure regime [17].

Equation (8) and (9) have been combined to yield the resonator Q in terms of the subjected temperature and pressure as

$$Q = a \cdot c(P_a)^b (T)^{\gamma} \tag{10}$$

The fitting is incorporated in the model as shown in [9].

[4] I(PLDN,PLATE) <+ ddt(Q(charge)); // Drained current by the actuator.
[5] value(total_force) <+ -Q(charge)*Q(charge)/(2*`P_EPS0*area); // Electrostatic force on the movable plate.
[6] value(total_force) <+ m*value(ext_accel); // External acceleration force.
[7] value(total_force) <+ -(sqrt(k_1*m)/value(Q_fac))*Vel(velocity); // Damping force.
[8] value(total_force) <+ -(k_1+k_tc*($temperature-298.15))*position_val; // Linear spring force contribution with temperature.
[9] value(Q_fac) <+ Q_lin*pow(value(Pressure),QPow_P)*pow($temperature,QPow_T)/pow(298.15,QPow_T); // Quality factor of the pressure sensor.

C. Resonator non-linearity

Non-linearity in these devices limit the maximum achievable short-term frequency stability for most applications. Duffing bifurcation instabilities are a result of Amplitude-frequency (A-f) dependence effects that limit the useful dynamic range available from these devices [14]. The lower limit of the range is set by the intrinsic noise in the MEMS system which has been elaborated in the next sub-section. The upper end of the dynamic range is limited by the resonator power handling capacity of the spring restoration force. Below this range, the vibrations are almost linear.

The non-linear spring force can be written as

$$F_{spring} = -k_1 z - k_3 z^3 \tag{11}$$

Here, in Equation (11), k_1 is the linear spring constant [8] and k_3 is the third order force non-linearity component [10]. From physics, we expect the unforced, undamped resonator to oscillate infinitely with constant amplitude at the resonance frequency f_r. However, owing to nonlinear forced vibrations i.e. nonlinear springs the peak frequency shifts to a higher or lower frequency depending on positive or negative k_3 respectively. For instance, with our device, at higher excitation levels, the resonance frequency shifts to a lower frequency with an increased vibration amplitude. Also, with nonlinear springs, the A-f relationship is then no longer a single-valued function and the resonator shows hysteresis [15].

D. Noise Considerations

As mentioned in the previous section, the lower end of the usable dynamic range of a micromechanical oscillator is set by the intrinsic noise in the MEMS system. Brownian motion has a high influence on the dynamic rage in micro-scale devices [14]. If the MEMS in in thermal equilibrium and the ambient temperature around a damped mechanical resonator is finite (i.e. not 0 K), the micromechanical resonator exhibits some degree of random Brownian motion. This constitutes the thermal noise in the mechanical domain which is dependent on the amount of damping in the MEMS. As the damping in our prototype resonator is mostly squeeze film damping due to the perpendicular motion of the movable membrane relative to the fixed substrate, the Brownian noise incorporated in the model is related to the damping of the system. The damping of the MEMS is computed in terms of the pressure sensor Q, according to the varying input pressure and temperature to the system. Associated with damping, there is a force noise generator, which is incorporated in the model [11].

$$F_{noise} = 4\, k_1 T \left(\frac{2\pi m f_r}{Q}\right) \tag{12}$$

E. Statistical Mismatch

The manufacturing variations or mismatch are of maximum importance during commercialization of the sensor. Having a good knowledge of them is of maximum importance to ensure a good manufacturing yield by means of designing electronics capable of compensate or tolerate such variations. In the model, the mismatch has been modeled as a change in the elastic constant and a change in the gap using a normal distribution random generator. This is enough for accounting for the main manufacturing variations found on resonators. As Verilog-A does not support Monte-Carlo simulations directly, a parameter named *mismatch* is used to determine if the nominal values are used or the statistically generated instead, as well as a means of initializing the seed of the normal random generator [12]. Inside the simulation environment (Cadence ADEXL, in our case) the parameter *mismatch* can be controlled from within the simulator itself.

III. Model Validation, Verification and Alignment

To validate the simulation results, the model parameters were extracted using Comsol simulations and the device measurements [12]. In the experimental setup, an Agilent 4294A precision impedance analyzer was used together with a custom-made vacuum probe station with a thermal chuck. More details of the experimental setup can be found in [12].

A. Static Capacitance Measurements

When driven with a constant voltage, the resonator plates will eventually snap together if the voltage applied is above the pull-in voltage V_p, causing a sharp increase of the plate capacitance. The pull-in voltage at which the resonator becomes unstable, is given by [16]

$$V_P = \left(\frac{8}{27}\frac{k_1 (z_0 - z)^3}{\varepsilon A}\right) \tag{13}$$

An accurate estimation of the pull-in voltage is critical in the design process of a MEMS resonator, as it represents a ratio of key mechanical parameters, as the elastic constant, the gap and the area. To find the values of those parameters, the following steps were done:

1. Obtaining the elastic constant k_1: The resonant frequency of the resonator is given by:

$$f_r = \frac{1}{2\pi}\sqrt{\frac{k_1}{m}} \tag{14}$$

As the resonator mass can easily be estimated from the layout, Equation (14) will allow us to extract the k_1 parameter.

[10] value(total_force) <+ -(k_3)*position_val*position_val*position_val; // Nonlinear spring force contribution.
[11] value(total_force) <+ white_noise(4*`P_K*$temperature*sqrt(k_1*m)/value(Q_fac), "Brownian"); // Brownian noise force.
[12] // In absence of a zero mismatch, the simulator generates a gaussian distribution of the returned values over a wide range
if (mismatch==0) k_1=k_1_mean; else k_1 = $rdist_normal(mismatch, k_1_mean, k_1_std);
if (mismatch==0) gap=gap_mean; else gap = $rdist_normal(mismatch, gap_mean, gap_std);

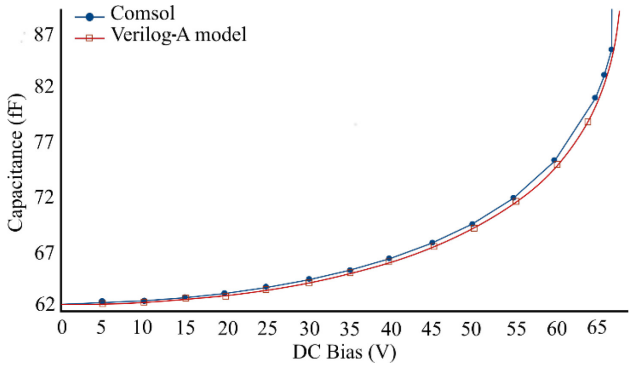

Fig. 3. Comparison of the capacitance vs. bias voltage characteristics of the CMOS-MEMS resonator obtained with a Comsol finite element analysis and the presented Verilog-A model.

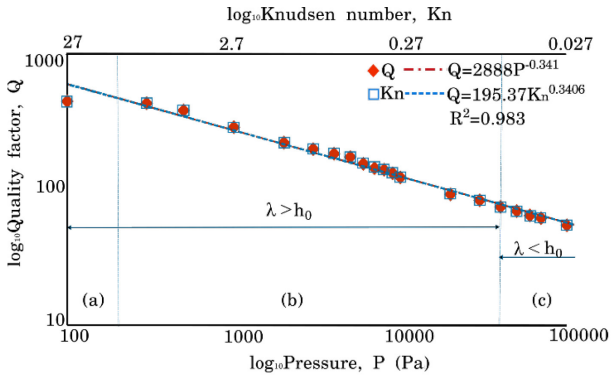

Fig. 4. Fitting of the quality factor vs. pressure characteristic of the CMOS-MEMS resonator. K_n scale is shown at the top over (a) molecular flow regime (b) transition flow regime (c) slip flow regime (see [12]).

2. Obtaining the gap (z_0-z): With the help of Comsol, and having the geometry of the resonator, the capacitance can be accurately estimated. By changing the gap in the simulator, an accurate gap value can be found that matches the measured pull-in voltage. Although a direct capacitance measurement can also be performed and then the gap extracted using equation (1), in our experience this method suffers from an increased error, probably due to the fringe and parasitic capacitances.

To validate the approach, a Comsol finite element analysis of the resonator was used to determine the capacitance vs. voltage relation, from zero volts to near the pull-in voltage, and then it was compared with the model result, as shown in **Fig. 3**. The obtained device pull-in from the model was 65 V, showing a close agreement with Finite Element Analysis (FEA) analysis with a convergence error of 3.08%.

B. Resonance and quality factor measurements

The damping coefficient of a resonator, which largely depends on the squeeze-film damping effects, varies with the air pressure according to Knudsen number (K_n) [12]. The experimental frequency response was obtained for pressures

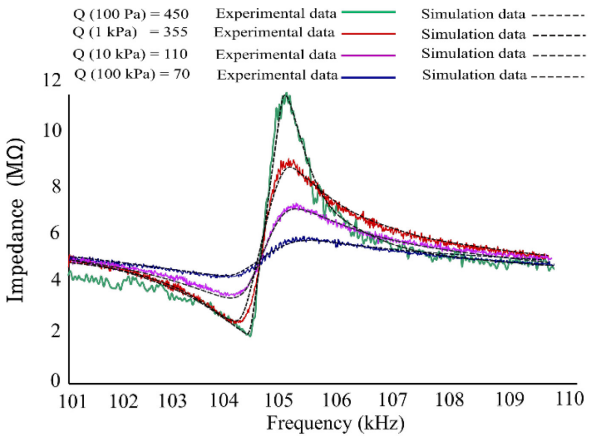

Fig. 5. Convergence of experimental measurements with simulation results of Verilog-A model for variable pressure regimes of 100 Pa, 1000 Pa, 10000 Pa and 101325 Pa.

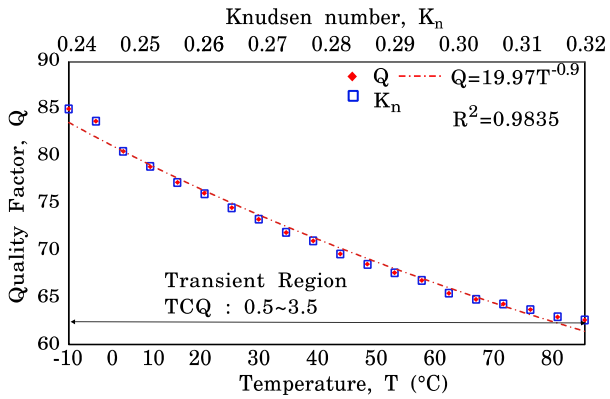

Fig. 6. Fitting of the experimental data of the CMOS MEMS resonator to illustrate the effect of temperature on Q at 30 kPa under variable temperatures

ranging from 100 Pa to 101325 Pa (atmospheric pressure) using the impedance analyzer. These measurements, however, are largely affected by the parasitic capacitance of the setup and the resonator. To mimic the parasitics effect, a capacitance was added in parallel with the MEMS model and its value adjusted to obtain the same static capacitive reading.

The quality factor (Q) was extracted from the measurements and plotted against the air pressure at a constant temperature, as shown in **Fig. 4**. Using log-log axes, a linear regression fit was calculated, allowing us to extract the parameters a and b of Equation (8), corresponding to the model parameters *QLin* and *QPow_P* respectively.

To verify the model, the resonance characteristic was measured using the impedance analyzer. Then, both parameters were incorporated in the model and simulated with the same pressures. When plotted together, an almost perfect fit is obtained, as shown in **Fig. 5**.

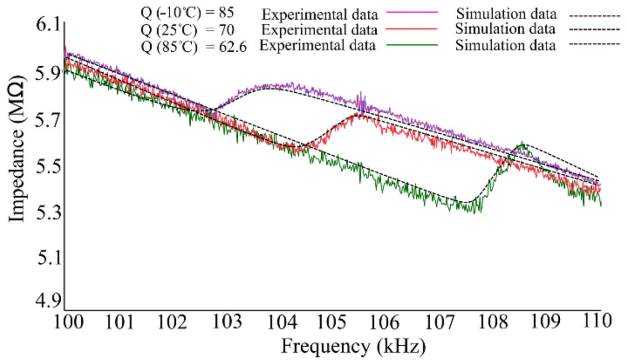

Fig. 7. Convergence of experimental measurements with simulation results for temperatures of -10 ºC, 25 ºC and 85 ºC at 30 kPa.

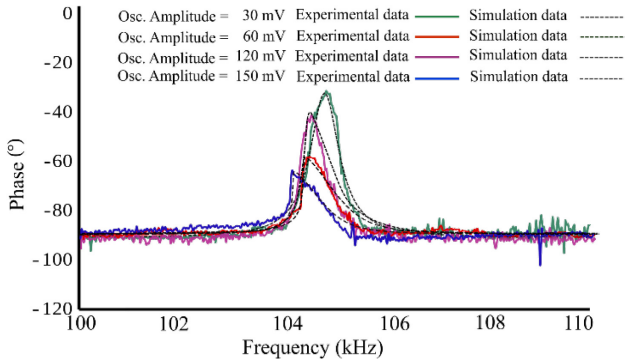

Fig. 8. Convergence of measurement data of resonator non-linearity with Verilog A model

C. *Convergence with Temperature Measurements*

Temperature disturbance is a vital concern in determination of the resonator *Q*. The experimental frequency response and thermal dependence data were recorded for the prototype resonator at variable conditions of temperatures ranging from -10 °C to 85 °C and a constant pressure of 30 kPa.

The pressure point was selected to observe distinct variations in resonance frequency at variable temperatures, taking into account several losses involved in the computation of the *Q*. The *Q* was extracted from the measurements and plotted against the temperatures at constant pressure, as shown in **Fig. 6**. According to characterization results, the resonance frequency was found to decrease with an increase in temperature due to the spring softening effect.

To align the experimental data with model simulations, the parameter *k_tc* was adjusted to have the same resonant-frequency temperature variations as in the measurements. Secondly, to correct for the variation of Q with temperature, the parameter *QPow_T* was adjusted for minimum divergence between the simulation and the measurements.

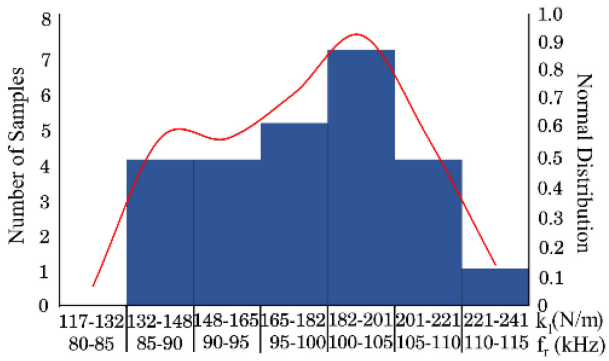

Fig. 9. Measured histogram of the resonator elastic constant or resonant frequency obtained with 25 samples.

The simulation results mimic the characterization results under variable environmental conditions to a considerable extent, as shown in **Fig. 7**, thus validating the reported model.

D. *Convergence with Nonlinearity Measurements*

To obtain the resonator nonlinearity k_3, the air pressure on the device was reduced to 30 kPa and several sweeps with increasing values of AC driving voltage were applied to the resonator while measuring its frequency response with the impedance analyzer. The combination of low pressure and increasing AC voltage led the resonator to oscillate with very high amplitudes, making the effect of the nonlinearity apparent. With one of these measurements k_3 was extracted by aligning the response with the simulator.

To verify the simulator response, the same value of k_3 was used to simulate the response for other values of driving voltage. As shown in **Fig. 8**, the model response shows a good match with the measurements. It should be noted that for making the simulator show the nonlinearities, a transient simulation needs to be done, as a regular AC simulation will show only the linear response because of its inherent response linearization.

E. *Convergence with Statistical Mismatch*

A total of twenty-five samples were measured to gives us a knowledge about the device variations. A histogram of the resonant frequency was obtained from the measurements, showing a range of 100 kHz to 105 kHz and a standard deviation of 2.753, as depicted in **Fig. 9**. The measured standard deviation was put in the model and the same value was obtained.

IV. Other Key Aspects

For proper functioning of the model, several key aspects must be also taken into consideration.

- *Simulator precision*: Our tests indicated that the simulator precision during a transient simulation must be increased with Q, otherwise, the energy stored in the resonator does not correspond to the Q of the resonator. A simulator control directive las used to automatically

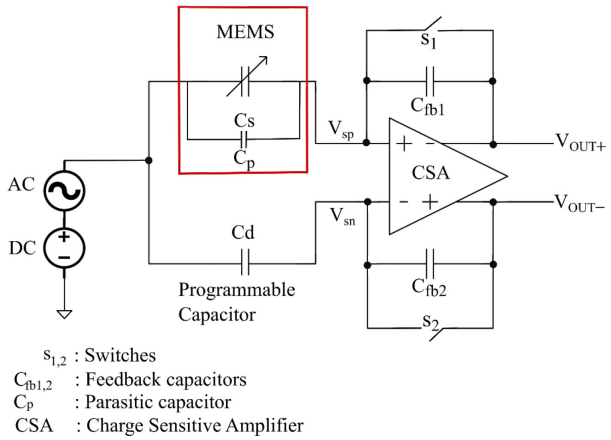

Fig. 10. Use of a Low-noise Amplifier as a test application to show MEMS co-simulation in electronic environment

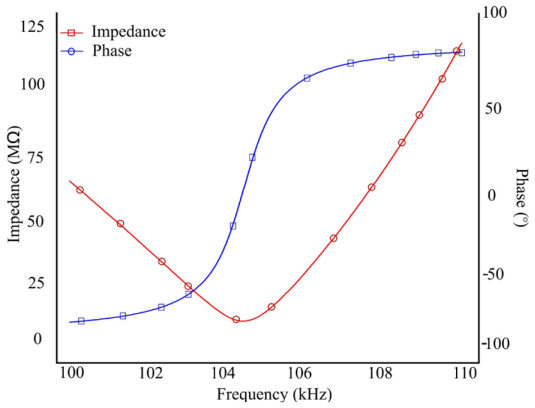

Fig. 12. Simulation of the pure resonance of the resonator obtained after parasitic cancellation of the resonator parasitic capacitance C_p, obtained by making the programmable capacitor $C_d \approx C_p$.

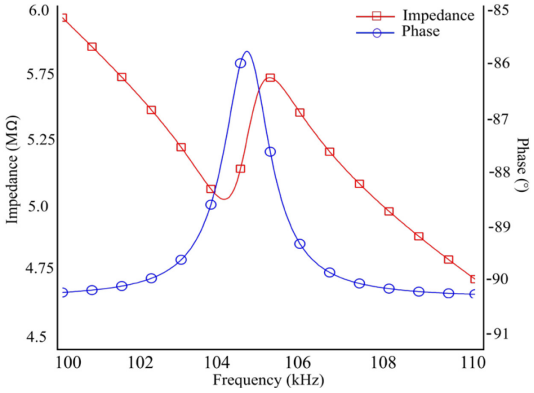

Fig. 11. Simulation of the native frequency response, amplitude and phase, of the resonator (in presence of its parasitic capacitance C_p).

set the maximum transient simulation step depending on the resonator quality factor [13].

- *Initial condition calculation (IC)*: As part of any transient simulation, the simulator tries to find the operating point of the circuit to shorten the simulation time. In this process, we have detected that frequently the gap of the MEMS becomes zero, hence crashing the simulator during the capacitance calculus. For avoiding this situation, the model instructs the simulator to take the parameter *gap_initial* as gap during the IC calculation [14].
- *Pull-in simulator crash*: The same error can occur during the simulation if the resonator plate voltage exceeds pull-in or an external force is applied that makes the gap zero or negative. To avoiding this error, the model forces the gap to be always larger than the minimum gap *gap_min* [15].
- *Stiction condition detection*: Stiction is a phenomenon involving the adhesion forces between the resonator plates. When the plates touch each other, they become stuck together unless a force of opposite sign appears, which can be the mechanical restoration force itself or externally applied. To have this effect present, a proximity condition is detected, which creates a force whenever the plates are touching [16].

V. Application Example: Charge Sensitive Amplifier with Parasitic Cancellation

After the alignment and verification phases, the resonator model was used within a co-simulation environment together with a transistor-level design of a low-noise charge sensitive amplifier (CSA) for detecting the capacitance (or position) change of the resonator [18]. The Cadence Design Suite was used together with the Spectre Simulator and the ADEXL simulation environment.

The top-level schematic of this application example has been illustrated in **Fig. 10**. The circuit utilizes a half-bridge fully differential capacitive feedback closed loop CTC (Continuous-Time Current mode) sensing amplifier. The usage of capacitors in the feedback path instead of resistors reduces the number of noisy components. A programmable capacitor C_d is connected to the inverting input of the CSA to reduce the effect of the MEMS resonator parasitic capacitance C_p.

[13] $bound_step(`M_TWO_PI*sqrt(m/k_1)/(precision_factor*value(Q_fac)); // Simulator precision must be increased with Q
[14] if(analysis("ic")) position_val=gap_initial; else position_val=Pos_MEMS(position); // Avoid crashing during IC calculation.
[15] position_val=((position_val<-(gap_val-gap_min)) ? -(gap_val-gap_min) : position_val); // Avoid the gap becoming zero
[16] if(position_val<=-(gap_val-1.01*gap_min)) status=1; else status=0; // Enable stiction adhesion forces if plates are touching.
if(status==1) stic_val=-stic; else stic_val=0;

The circuit has two operating phases:

a. *Reset Phase*: The feedback switches ($s_{1,2}$) are closed and the operational amplifier inputs and outputs are shorted. This resets the feedback capacitors $C_{fb1,2}$ and provides DC stability of the circuit. In this mode, the differential output voltage $V_{OUT}=0$.
b. *Measurement Phase*: The switches are open and only the capacitive feedback works as the feedback net. Provided that no AC excitation is present, the output voltage of the amplifier is then

$$V_{OUT} = V_{DC}\frac{\Delta C}{C_{fb}} \tag{13}$$

where ΔC is the resonator capacitance variation. The frequency response of the resonator can be obtained by sweeping the frequency of the AC voltage source. However, this measurement is affected by the signal transfer of the resonator parasitic capacitance C_p. Due to the usual small signals involved with the MEMS resonators, the effect of the parasitic can easily overcome or severely distort the measurement, as shown in **Fig. 11**. The phase rotation of the resonator reaches only 4º, instead of the full 180º that we can expect from a pure resonator, and the impedance shows a limited change and a spurious positive peaking, known as antiresonance [19].

To recover a pure resonance, the same circuit of **Fig. 10** can be used, if the value of the programmable capacitor C_d is adjusted to become similar to the parasitic capacitor C_p. In this case, the currents from C_p and C_d both cancel each other, leaving only the current of the resonator, as shown in **Fig. 12**.

VI. CONCLUSION

We have successfully developed a second order non-linear behavioral model adequate for co-simulation within the Cadence microelectronic design tools that emulates the realistic behavior of a CMOS-MEMS resonator. Besides of the second-order resonator behavior, this model includes the effects of temperature, noise, nonlinearity and mismatch. A parameter extraction method based in the experimental measurements has also been presented, as well as a comparison between the measurements and the model simulation results. This comparison shows an accurate prediction of the resonator response outside the alignment points, including pressure ranges between 100 Pa and 100 kPa, temperature ranges from -10 ºC to 85 ºC and severe levels of voltage overdrive to create nonlinearities. The model has also been co-simulated with a charge sensitive amplifier implemented at transistor-level inside the Cadence design suite, implementing a parasitic cancellation application useful to obtain a pure resonance.

It is expected that this second-order behavioral model serves both as an advanced resonator model compatible with microelectronic design tools and as a tutorial for creating similar models for MEMS or microelectronics designers requiring a model capable of close interaction the ASIC design tools.

REFERENCES

[1] O. Leman, N. Dumas, F. Mailly, L. Latorre, and P. Nouet, "An approach to integrate MEMS into high-level system design flows," *2008 Jt. IEEE North-East Work. Circuits Syst. TAISA Conf. NEWCAS-TAISA*, pp. 273–276, 2008.

[2] Q. Jing, T. Mukherjee, and G. K. Fedder, "Schematic-based lumped parameterized behavioral modeling for suspended MEMS," in *Proceedings of the 2002 IEEE/ACM international conference on Computer-aided design - ICCAD '02*, 2002, pp. 367–373.

[3] S. D. Senturia, N. Aluru, and J. White, "Simulating the behavior of MEMS devices: Computational methods and needs," *IEEE Comput. Sci. Eng.*, vol. 4, no. 1, pp. 30–43, 1997.

[4] N. Bushyager, M. M. Tentzeris, L. Gatewood, and J. Denatale, "A Novel Adaptive Approach to Modeling MEMS Tunable Capacitors Using MRTD and FDTD Techniques," *Spring*, vol. 0, no. C, pp. 0–3, 2001.

[5] G. K. Fedder, "Top-down design of MEMS," *2000 Int. Conf. Model. Simul. Microsystems - MSM 2000*, vol. 10, pp. 7–10, 2000.

[6] I. A. Ali, "Modeling and simulation of MEMS components : challenges and possible solutions," *Micromach. Tech. Fabr. Micro Nano Struct.*, pp. 277–301, 2012.

[7] C. C. McAndrew *et al.*, "Best Practices for Compact Modeling in Verilog-A," *IEEE J. Electron Devices Soc.*, vol. 3, no. 5, pp. 383–396, 2015.

[8] C. Guo and G. K. Fedder, "Behavioral modeling of a CMOS-MEMS nonlinear parametric resonator," *J. Microelectromechanical Syst.*, vol. 22, no. 6, pp. 1447–1457, 2013.

[9] G. Zhou and P. Dowd, "A method to include micromechanical components into the system level simulation," *Sensors Actuators, A Phys.*, vol. 97–98, pp. 386–397, 2002.

[10] C. Mandelbaum *et al.*, "Behavioral Modelling and Simulation of micromechanical resonator for communications applications ," Symposium on Design, Test, Integration and Packaging of MEMS/MOEMS , pp. 21–26, 2003.

[11] S. Lee, M. U. Demirci, and C. T.-C. Nguyen, "A 10-MHz Micromechanical Resonator Pierce Reference Oscillator for Communications," *IEEE Int. Solid-State Sensors Actuators Conf.*, vol. 2, pp. 1094–1097, 2001.

[12] L. Khine and M. Palaniapan, "Behavioural modelling and system-level simulation of micromechanical beam resonators," *J. Phys. Conf. Ser.*, vol. 34, pp. 1053–1058, 2006.

[13] S. Banerji, P. Michalik, D. Fernández, J. Madrenas, A. Mola, and J. Montanyà, "CMOS-MEMS resonant pressure sensors: optimization and validation through comparative analysis," *Microsyst. Technol.*, pp. 1–17, 2016.

[14] V. Kaajakari, T. Mattila, A. Oja, and H. Seppä, "Nonlinear limits for single-crystal silicon microresonators," *J. Microelectromechanical Syst.*, vol. 13, no. 5, pp. 715–724, 2004.

[15] V. Kaajakari, "MEMS Tutorial : Nonlinearity in Micromechanical Resonators," *MEMS Mater. Kaajakari*, pp. 1–7, 2009.

[16] V. Kaajakari, "MEMS Tutorial: Pull-In Voltage in Electrostatic Microactuators," *Pract. MEMS*, no. 5, pp. 1–2, 2009.

[17] S. Banerji, J. Madrenas, and D. Fernandez, "Temperature and pressure characterization of the quality factor in a CMOS-MEMS resonator," *2016 IEEE Sensors*, no. c, pp. 1–3, 2016.

[18] J. M. Sánchez-Chiva, P. Michalik, D. Fernández and J. Madrenas, "A CMOS BEOL accelerometer low-noise readout amplifier with 4.2 zF/√Hz total noise floor," 2015 IEEE Sensors Conference, Busan, 2015, pp. 1765–1768, 2015.

[19] M. Lerman and D. Elata, "On the quality-factor of micro-resonators," in *Procedia Engineering*, 2010, vol. 5, pp. 95–98.

[20] D. Fernández, J. Ricart, and J. Madrenas, "Experiments on the release of CMOS-micromachined metal layers," *J. Sensors*, vol. 2010, 2010.

[21] P. Michalik, J. M. Sánchez-Chiva, D. Fernández and J. Madrenas, "CMOS BEOL-embedded z-axis accelerometer," *Electron. Lett.*, vol. 51, no. 11, pp. 865–867, 2015.

Saoni Banerji was born in Bokaro Steel City, India, in 1989. She received the B.Tech. degree in Electrical and Electronics engineering in 2011, M.Sc. degree in Electronics from Nanyang Technological University, Singapore in 2014, and Diploma in Business Management from London School of Business and Finance (LSBF) in April 2017. She is currently pursuing her PhD in the fields of MEMS design and circuits, and designing control architectures for MEMS Sensors signal conditioning in Universitat Politècnica de Catalunya (UPC), Barcelona, Spain. Her current research interests and competencies include MEMS modeling, design of signal conditioning architectures with CMOS processes, testing and characterization of CMOS-MEMS devices. Since August 2017, she is working in Nanusens, gaining experience with finite element simulations, characterization and measurements of CMOS-MEMS accelerometers.

Daniel Fernández was born in Barcelona, Spain, in 1979. He received the M.Sc. degree in telecommunications engineering, Ph.D. degree (cum laude), and M.B.A. degree from Universitat Politècnica de Catalunya (UPC), Barcelona, Spain, in 2004, 2008 and 2009, respectively. From 2008 to 2010 he worked as a Postdoctoral Researcher at the Electronic Engineering Department, UPC in the fields of CMOS surface micromachining, circuits and control architectures for MEMS sensors and actuators, trans linear circuits for analog signal processing and digital implementations of power converters. From 2010 to 2014 he worked as Principal ASIC Engineer at Baolab Microsystems developing circuits and architectures for CMOS MEMS/NEMS-based products, and as ASIC Design Engineer Contractor for the European Space Agency designing radiation-hardened integrated-circuits and interface blocks for space exploration in interplanetary missions. Currently he is Chief Technology and Science Officer at Nanusens, Cerdanyola Del Vallès, Spain, where he works towards the development of innovative circuits and architectures for MEMS sensors signal conditioning.

Jordi Madrenas (Telecom. Eng. ’86, Ph.D. ’91, UPC, Barcelona, Catalunya, Spain) is currently Associate Professor at the Department of Electronic Engineering, Technical University of Catalunya (UPC BarcelonaTech). He has participated in 5 European projects and coordinated 6 Spanish national research projects. Also, he has coordinated several contracts with companies. At present, he coordinates a national project on MEMS on-chip and microsensor bio-inspired signal processing. He has co-authored more than 150 scientific journal and international conference papers, two books and 5 book chapters. Between 2000 and 2003 he was Vice-Dean of Studies of the Telecommunication Engineering School of Barcelona, UPC. His current research interests include analog, mixed-signal and digital VLSI and FPGA design, CMOS-MEMS design and conditioning, ultra-low-power design, bioinspired/neuromorphic system implementation and rad-hard mixed-signal circuits.